DIRECT NUMERICAL SIMULATION OF PASSIVE SCALAR TURBULENT FIELDS WITH WALL SCALAR FLUCTUATIONS AT LOW, MEDIUM AND HIGH PRANDTL NUMBERS

B. Chaouat

ONERA, Université Paris-Saclay, 92322 Châtillon, France

bruno.chaouat@onera.fr

Abstract

Direct numerical simulation of passive scalar turbulent fields subjected to constant time-averaged fluxes is performed with and without wall scalar fluctuations for several Prandtl numbers. It is found that the half-scalar variance, dissipation and molecular diffusion processes are highly influenced by the wall scalar fluctuations but not the redistribution process associated with the pressure scalar-gradient correlation.

1 Introduction

Turbulent flows involving the transport of passive scalar are of major importance in many engineering applications and in nature like for instance the pollution dispersal in atmosphere. In various flow configurations involving heat transfer between impermeable walls like for instance liquid metal-cooled reactors, the temperature fluctuations at the wall are not reduced to zero and may lead to thermal fatigue failure of solid structures. Considering that the temperature fluctuations play an important role in industrial devices, the objective of this paper is to perform direct numerical simulation (DNS) of turbulent channel flows to investigate the effect of the wall-scalar fluctuations on scalar fields (Tiselj at al,, 2001; Flageul et al. 2015, Chaouat and Peyret, 2019). Simulation are worked out for the Reynolds number $R_\tau = u_\tau \delta/\nu = 395$ based on the friction velocity u_τ, the channel half-width δ and the molecular viscosity ν, and the Prandtl numbers $P_r = 0.1$, 1 and 10. A special interest is devoted to the budget of the scalar variance k_θ^+ and the turbulent scalar fluxes $\tau_{i\theta}^+$. This DNS database will be useful to validate turbulence models with heat transfer (Schiestel, 2008, Hanjalic and Launder, 2011; Chaouat, 2017; Schiestel and Chaouat, 2022).

2 Equations, boundary conditions and numerical procedure

The momentum equation reads

$$\frac{\partial u_i^+}{\partial t^+} + \frac{\partial}{\partial x_j^+}(u_i^+ u_j^+) = -\frac{\partial p^+}{\partial x_i^+} + \frac{1}{R_\tau}\frac{\partial^2 u_i^+}{\partial x_j^+ \partial x_j^+} + G_i \tag{1}$$

where u_i and p denote the velocity and pressure, respectively, the coordinate and flow variables are normalized by δ, the friction velocity u_τ, the kinematic viscosity ν and constant density ρ. The quantity $G_i = \delta_{1i}$ is the source term to get periodic condition. As the mean scalar variable $\langle\Theta\rangle$ increases linearly in the x_1 direction, a change of variable is made by introducing the new scalar variable $\theta = x_1 \partial\langle\Theta_m\rangle/\partial x_1 - \Theta$ (Kozuka et al., 2009). The transport equation for the passive scalar θ reads

$$\frac{\partial \theta^+}{\partial t^+} + \frac{\partial}{\partial x_j^+}(\theta^+ u_j^+) = \frac{1}{R_\tau P_r}\frac{\partial^2 \theta^+}{\partial x_j^+ \partial x_j^+} + Q \tag{2}$$

where $Q = -u_1^+/U_b^+$ denotes the source term, U_b^+ is the bulk velocity. The variable θ is normalized by $\theta_\tau = q_w/(\rho c_p u_\tau)$ where ρ, c_p and q_w are the fluid density, the specific heat at constant pressure and the heat flux at the wall. The heat flux is $q_w = -\kappa(\partial\theta/\partial x_3)_w$ where κ stands for the thermal conductivity $\kappa = \rho c_p \nu/P_r$. The thermal diffusivity is $\sigma = \kappa/(\rho c_p) = \nu/P_r$.

Boundary conditions

The flow solution at the interface for the solid-fluid conjugate system depends on the thermal effusivity ratio of the gas to the solid given by $K = a/a_w$ where $a = \sqrt{\rho c_p \kappa}$ involving the density ρ, the specific heat at constant pressure c_p, and the scalar conductivity κ, the subscript w referring to the properties of the wall. Usually, the ratio of the effusivity of gas to the one of structural materials is very small $K \leq 10^{-3}$ but not for liquids where it is of order unity (Kasagi et al. 1989). For a turbulent flow subjected to heat fluxes through the wall, two limiting boundary conditions can be considered depending on the fluid and solid properties. The first one is the isoscalar boundary condition with a constant wall scalar (case I) implying that its fluctuation at the wall θ'_w and its *rms* $\langle\theta'\theta'\rangle_w$ are zero and corresponds to the usual case where $K \ll 1$, i.e., $a \ll a_w$ with a large wall thickness at the interface. The second one is the isoflux boundary condition implying non-zero scalar fluctuations at the wall (case II) and corresponds to the case where $K \gg 1$, i.e., $a \gg a_w$ with an infinitesimal wall thickness, the derivative $(\partial\theta'_w/\partial x_n)_w$ along the normal direction to the wall x_n is zero because $q'_w = 0$ leading to $(\partial \langle\theta'\theta'\rangle / \partial x_n)_w = 0$.

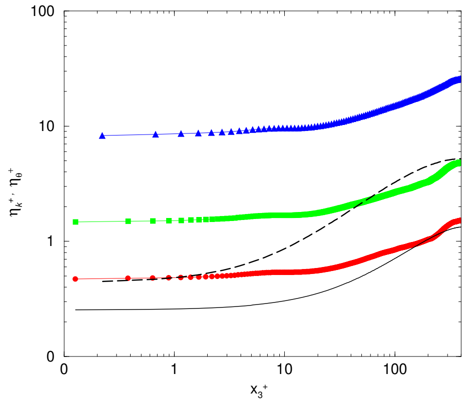

Figure 1: Kolmogorov and Batchelor length-scales η_κ^+, η_θ^+ computed for the Prandtl numbers $P_r = 0.1$, 1 and 10 - - -: $\Delta_3^+(M_1)$; —: $\Delta_3^+(M_2)$; ▲: η_θ^+ ($P_r = 0.1$); ■ $\eta_\theta^+ = \eta_\kappa^+$ ($P_r = 1$); ●: η_κ^+ ($P_r = 10$). $R_\tau = 395$.

Numerical procedure

The dimension of the channel in the streamwise, spanwise and normal directions along the x_1, x_2, x_3 axes are $L_1 = 6.4\delta$, $L_2 = 3.2\delta$ and $L_3 = 2\delta$. For the Reynolds and Prandtl number values studied here, the number of grid points varies from the mesh M_1 of resolution $512 \times 256 \times 512$ for $P_r = 0.1$ and 1 to M_2 of extremely high resolution $1024 \times 512 \times 1024$ for $P_r = 10$. The grid refinement allows to solve both the Kolmogorov scale $\eta_\kappa = (\nu^3/\epsilon)^{1/4}$ and the Batchelor length-scale η_θ (Batchelor, 1959; Tennekes and Lumley, 1972) which approaches η_κ at P_r of order of unity, $\eta_\theta = (\sigma^3/\epsilon)^{1/4} = \eta_\kappa/P_r^{3/4}$ at small Prandtl numbers and $\eta_\theta = (\nu\sigma^2/\epsilon)^{1/4} = \eta_\kappa/P_r^{1/2}$ at large Prandtl numbers as shown in Figure 1. The equations are integrated in time using an explicit Runge-Kutta scheme of fourth order accuracy in time and solved in space by means of a centered scheme of fourth order accuracy in space. The CFD code (Chaouat, 2011) is based on the finite volume technique and is optimized with message passing interface (MPI).

3 Numerical results

Figure 2 is a snapshot view of the scalar field θ in the (x_1, x_3) mid-plane for the Prandtl number $P_r = 10$. This figure highlights substantial detachment of swirling vortex elements growing from the boundary layer to the central region of the channel along the normal direction to the wall. Figure 3 shows the contours plots of the instantaneous scalar field θ in the (x_1, x_3) mid-plane, respectively, for the Prandtl numbers $P_r = 0.1$, 1 and 10. It is found that the topology of these structures considerably changes as the Prandtl number increases from $P_r = 0.1$ to 10. Indeed, these structures get thinner because of the important decrease of the Batchelor length-scale η_θ according to the power law $\eta_\theta = \eta_\kappa/P_r^{1/2}$. They are relatively smooth and organized with dominant large scales at the lower Prandtl number $P_r = 0.1$ but become more and more chaotic as the Prandtl number increases from 0.1 to 10, the gradients being sharper.

Mean scalar and half-scalar variance

Previous simulations (Chaouat and Peyret, 2019) have shown that the mean scalar $\langle\theta^+\rangle$ remains not affected by the wall scalar fluctuations but in the contrary, the half scalar variance $k_\theta^+ = \langle\theta'^+\theta'^+\rangle/2$ is highly impacted essentially in the near wall region. For instance, Figure 4 illustrates the *rms* fluctuation intensities for $P_r = 1$ indicating a change in the immediate vicinity of the wall. As expected, the *rms* reduces to zero for the isoscalar boundary condition (case I) but not for the isoflux boundary condition (case II) where it is relatively high satisfying the wall condition $(\partial \langle\theta'\theta'\rangle / \partial x_n)_w = 0$.

Transport equation for the half-scalar variance

The budget terms appearing in the transport equation for the half-scalar variance k_θ^+ are non-dimensionalized by the factor $u_\tau^2\theta_\tau^2/\nu$. The transport equation for k_θ^+ reads

$$0 = \tau_{1\theta}^+ \frac{\partial \langle\Theta_m^+\rangle}{\partial x_1^+} - \tau_{j\theta}^+ \frac{\partial \langle\theta^+\rangle}{\partial x_j^+} - \frac{\partial}{\partial x_j^+} \langle u_j'^+ \theta'^{+2}\rangle + \frac{1}{P_r}\frac{\partial^2 k_\theta^+}{\partial x_j^{2+}} - \frac{1}{P_r}\left\langle \frac{\partial\theta'^+}{\partial x_j^+}\frac{\partial\theta'^+}{\partial x_j^+}\right\rangle \quad (3)$$

where the terms appearing in this equation are the production P_θ^+, the turbulent diffusion due to the correlation of the scalar-velocity T_θ^+, the molecular diffusion d_θ^+ and the dissipation-rate ϵ_θ^+ of the half-scalar variance k_θ^+. The first production term is negligibly small compared with the second term because $\partial\langle\Theta_m^+\rangle/\partial x_1^+ \ll \partial\langle\theta^+\rangle/\partial x_3^+$. Figure 5 shows the budget of the transport equation for the scalar variance k_θ^+. The curves are somewhat flattened for $P_r = 0.1$ but become very sharp for $P_r = 10$ and also their peak move closer to the wall as the Prandtl number increases. The dominant processes in the central region of the channel are the production as a gain term and the dissipation rate as a sink term that balance each other at all Prandtl numbers. The viscous and turbulent diffusion terms are of appreciable magnitude in the very near wall region showing that they both play an important role in the transfer of the passive scalar. It appears that the dissipation-rate term ϵ_θ^+ and the viscous diffusion term d_θ^+ are still of the same order of magnitude away from the wall but they are significantly smaller in the vicinity of the wall for case II in comparaison with case I. The other terms such as the production P_θ^+ and the turbulent diffusion T_θ^+ remain relatively unaffected by the type of boundary condition, although the turbulent diffusion T_θ^+ is however slightly attenuated

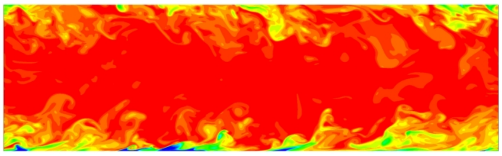

Figure 2: Snapshot view of the scalar field θ in the (x_1, x_3) mid-plane. $\theta'_w = 0$ (case I). $P_r = 10$.

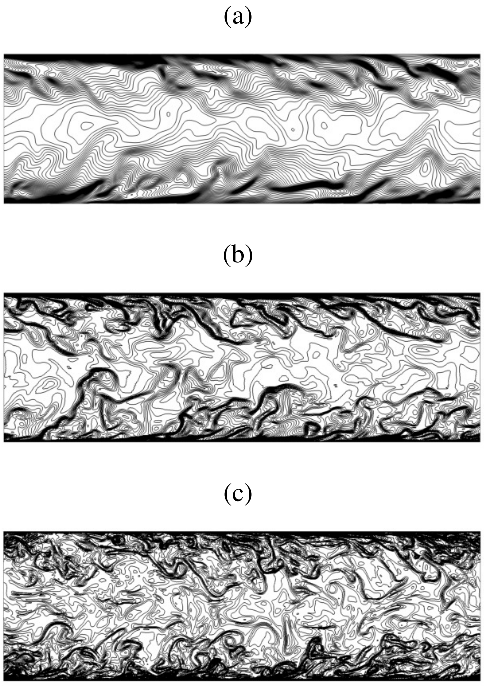

Figure 3: Contours of the instantaneous scalar field θ in the (x_1, x_3) mid-plane. $\theta'_w = 0$ (case I). (a) $P_r = 0.1$. (b) $P_r = 1$; (c) $P_r = 10$.

in the near wall region.

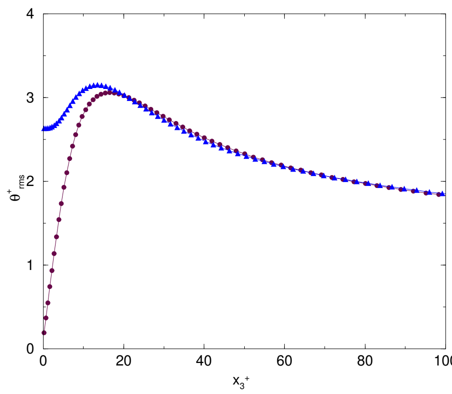

Figure 4: Root-mean square of the scalar variance $\theta^+_{rms} = \sqrt{\langle \theta'^+ \theta'^+ \rangle}$ versus the wall unit distance. $\theta'_w = 0$ (case I), $\bullet$. $q'_w = 0$ (case II), $\blacktriangle$. (c) $P_r = 1$; $R_\tau = 395$.

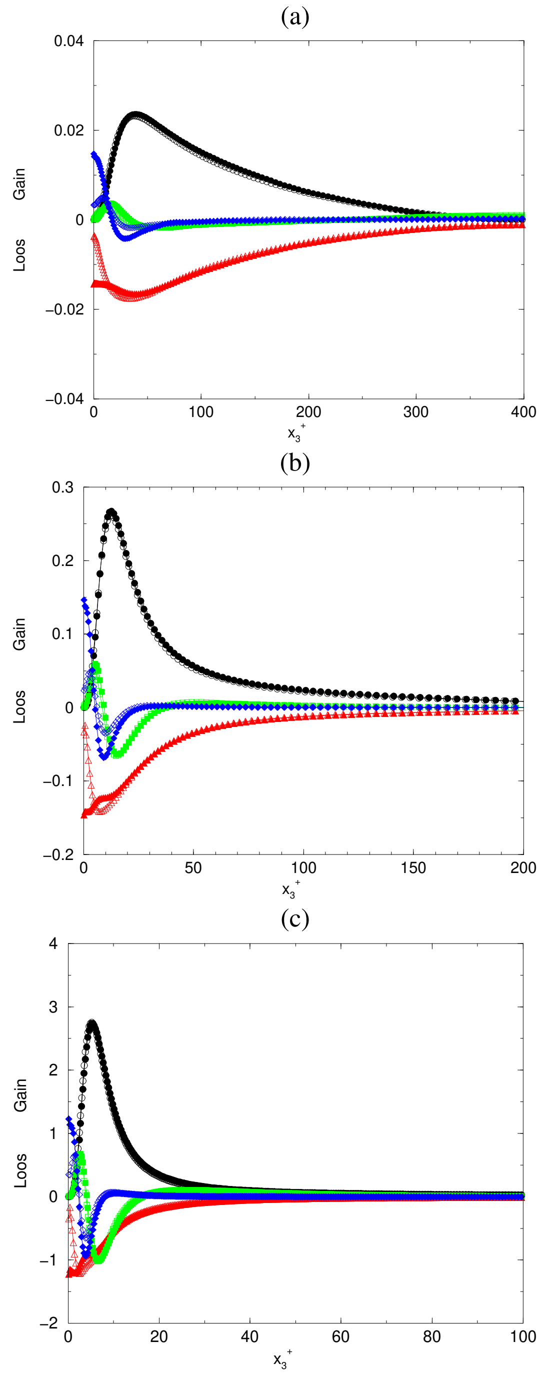

Figure 5: Budget of the transport equation for the scalar variance k^+_θ versus the wall unit distance. $\theta'_w = 0$, $\bullet$: P^+_θ; $\blacktriangle$: ϵ^+_θ; $\blacklozenge$: d^+_θ; $\blacksquare$: T^+_θ. $q'_w = 0$, $\circ$: P^+_θ; $\triangle$: ϵ^+_θ; $\lozenge$: d^+_θ; $\square$: T^+_θ. (a) $P_r = 0.1$; (b) $P_r = 1$; (c) $P_r = 10$; $R_\tau = 395$.

Transport equation for the scalar fluxes

The budget terms are non-dimensionalized by the factor $u^3_\tau \theta_\tau / \nu$. The transport equation for the turbu-

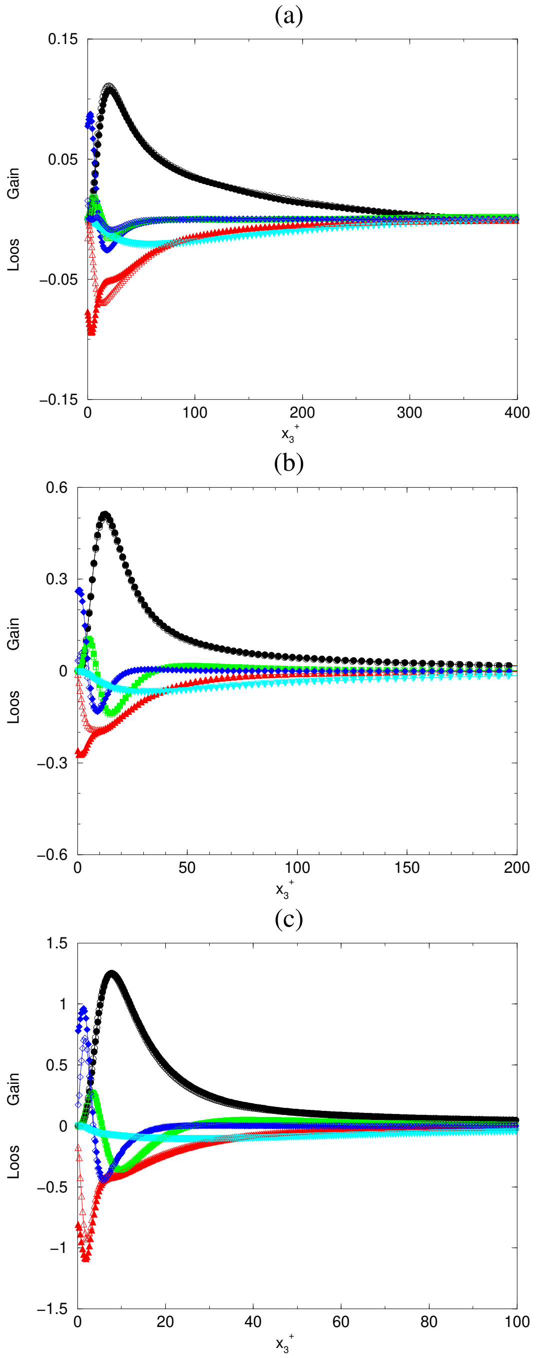

Figure 6: Budget of the transport equation for the streamwise turbulent scalar flux $\tau_{1\theta}^+$ versus the wall unit distance. $\theta'_w = 0$, ●: $P_{1\theta}^+$; ▲ : $\epsilon_{1\theta}^+$; ◆ : $d_{1\theta}^+$; ■ : $T_{1\theta}^+$; ▼ : $\Pi_{1\theta}^+$. $q'_w = 0$, ○: $P_{1\theta}^+$; △ : $\epsilon_{1\theta}^+$; ◇ : $d_{1\theta}^+$; □ : $T_{1\theta}^+$. ▽ : $\Pi_{1\theta}^+$. (a) $P_r = 0.1$; (b) $P_r = 1$; (c) $P_r = 10$; $R_\tau = 395$.

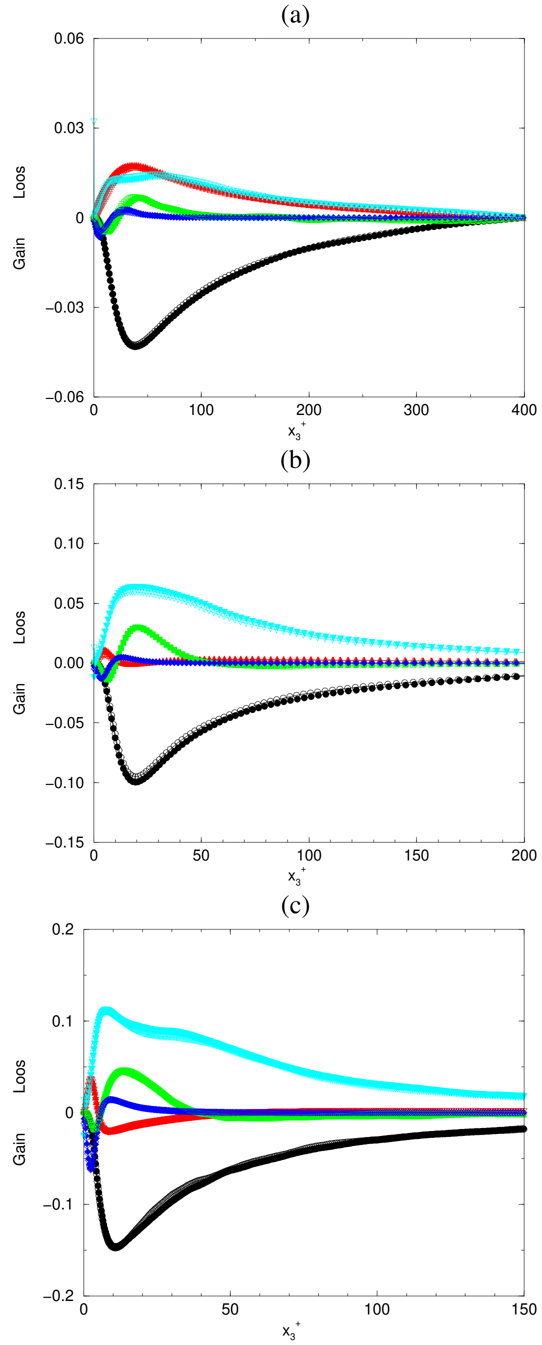

Figure 7: Budget of the transport equation for the wall-normal turbulent scalar flux $\tau_{3\theta}^+ = \langle u_3'^+ \theta'^+ \rangle$ versus the wall unit distance. $\theta'_w = 0$, ●: $P_{3\theta}^+$; ▲ : $\epsilon_{3\theta}^+$; ◆ : $d_{3\theta}^+$; ■ : $T_{3\theta}^+$; ▼ : $\Pi_{3\theta}^+$. $q'_w = 0$, ○: $P_{3\theta}^+$; △ : $\epsilon_{3\theta}^+$; ◇ : $d_{3\theta}^+$; □ : $T_{3\theta}^+$. ▽ : $\Pi_{3\theta}^+$. (a) $P_r = 0.1$; (b) $P_r = 1$; (c) $P_r = 10$; $R_\tau = 395$.

lent scalar flux $\tau_{i\theta}^{+} = \left\langle u_i'^{+}\theta'^{+}\right\rangle$ reads

$$
\begin{aligned}
0 &= \tau_{1i}^{+}\frac{\partial\left\langle\Theta_m^{+}\right\rangle}{\partial x_1^{+}} - \tau_{ij}^{+}\frac{\partial\left\langle\theta^{+}\right\rangle}{\partial x_j^{+}} - \tau_{j\theta}^{+}\frac{\partial\left\langle u_i^{+}\right\rangle}{\partial x_j^{+}} \\
&- \frac{\partial}{\partial x_j^{+}}\left\langle u_i'^{+}u_j'^{+}\theta'^{+}\right\rangle + \frac{\partial}{\partial x_j}\left\langle\theta'^{+}\frac{\partial u_i'^{+}}{\partial x_j^{+}}\right\rangle \\
&+ \frac{1}{P_r}\frac{\partial}{\partial x_j}\left\langle u_i'^{+}\frac{\partial\theta'^{+}}{\partial x_j^{+}}\right\rangle - \left\langle\theta'^{+}\frac{\partial p'^{+}}{\partial x_i^{+}}\right\rangle \\
&- \left(1+\frac{1}{P_r}\right)\left\langle\frac{\partial u_i'^{+}}{\partial x_j^{+}}\frac{\partial\theta'^{+}}{\partial x_j^{+}}\right\rangle
\end{aligned} \tag{4}
$$

where in this equation, $\tau_{ij}^{+} = \left\langle u_i'^{+}u_j'^{+}\right\rangle$. The terms appearing in this equation are the production, $P_{i\theta}^{+(1)}$, $P_{i\theta}^{+(2)}$ and $P_{i\theta}^{+(3)}$, the turbulent diffusion $T_{i\theta}^{+}$, the viscous and molecular diffusion, $d_{i\theta}^{+(1)}$ and $d_{i\theta}^{+(2)}$, the scalar-pressure gradients $\Pi_{i\theta}^{+}$, and the scalar dissipation $\epsilon_{i\theta}^{+}$. Figure 6 displays the evolution of the streamwise turbulent scalar flux $\tau_{1\theta}^{+}$ versus the wall distance. The main contribution of the production are $P_{1\theta}^{+(2)} = -\tau_{13}^{+}\partial\left\langle\theta^{+}\right\rangle/\partial x_3^{+}$ and $P_{1\theta}^{+(3)} = -\tau_{3\theta}^{+}\partial\left\langle u_1^{+}\right\rangle/\partial x_3^{+}$ involving the interaction between the turbulent shear stress and the mean scalar gradient as well as the interaction between the wall-normal turbulent scalar flux and the mean streamwise velocity gradient. The dissipation term $\epsilon_{1\theta}^{+}$ remains large all over the channel cross-section due to the high correlation of the fluctuating velocity-scalar gradients $\left\langle\left(\partial u_1'^{+}/\partial x_j^{+}\right)\left(\partial\theta'^{+}/\partial x_j^{+}\right)\right\rangle$. It is found that the curves corresponding to the different terms appearing in (4) are departing further in the wall region but start to merge as the wall distance increases from the wall. The dissipation-rate and molecular diffusion terms are considerably attenuated at the wall. Moreover, the scalar-pressure gradients $\Pi_{1\theta}^{+}$ remains not affected by the wall scalar fluctuations for all Prandtl numbers. Figure 7 exhibits the evolution of the wall-normal turbulent scalar flux $\tau_{3\theta}^{+}$ versus the wall distance. The production term $P_{3\theta}^{+}$ appearing in (4) is here mainly governed by the two terms $P_{3\theta}^{+(2)} = -\tau_{33}^{+}\partial\left\langle\theta^{+}\right\rangle/\partial x_3^{+}$ and $P_{3\theta}^{+(3)} = -\tau_{3\theta}^{+}\partial\left\langle u_3^{+}\right\rangle/\partial x_3^{+}$ involving the interaction of the wall-normal turbulent stress τ_{33}^{+} with the mean scalar gradient as well as the interaction between the wall-normal turbulent scalar flux with the mean normal velocity gradient. The scalar dissipation-rate $\epsilon_{3\theta}^{+}$ is caused by the correlation of the fluctuating velocity-scalar gradients $\left\langle\left(\partial u_j'^{+}/\partial x_j^{+}\right)\left(\partial\theta'^{+}/\partial x_j^{+}\right)\right\rangle$ while the scalar pressure gradient correlation term is computed as $\Pi_{3\theta}^{+} = -\left\langle\theta'^{+}\partial p'^{+}/\partial x_3^{+}\right\rangle$. For all Prandtl numbers, the production is here negative, while the dissipation-rate as well as the pressure gradient correlation terms are positive. It appears that the scalar-pressure gradient correlation term $\Pi_{3\theta}^{+}$ gradually increases as the Prandtl number increases so that it contributes more significantly to the budget. The budget for $\tau_{3\theta}$ highly depends on the Prandtl number. For $P_r = 0.1$, $P_{3\theta}^{+}$ balance with the two sink terms $\Pi_{3\theta}^{+}$ and $\epsilon_{3\theta}^{+}$ whereas for $P_r = 10$, $P_{3\theta}^{+}$ roughly balances with $\Pi_{3\theta}^{+}$ that becomes dominant among the other terms. This result show that the contribution of the scalar-pressure gradient correlation term $\Pi_{3\theta}^{+}$ is essential and cannot be ignored in the budget equation. At a first sight, no apparent differences between the curves associated with and without wall scalar fluctuations are visible from the wall to the centerline of the channel.

4 Turbulent fluxes

The knowledge of the turbulent scalar fluxes $\tau_{i\theta} = \langle u_i'\theta'\rangle$ is of particular interest in mass and heat transfer. In eddy viscosity models (EVM), it is computed assuming a gradient hypothesis (Hanjalic and Launder, 2011)

$$
\tau_{i\theta} = -\frac{\nu_t}{Pr_t}\frac{\partial\langle\theta\rangle}{\partial x_i} \tag{5}
$$

where Pr_t is the turbulent Prandtl number and ν_t denotes the turbulent viscosity. The turbulent Prandtl number is defined itself as the ratio of the turbulent eddy viscosity ν_t to the turbulent eddy diffusivity σ_t as

$$
Pr_t = \frac{\nu_t}{\sigma_t} = \frac{\tau_{13}}{\tau_{3\theta}}\frac{\partial\langle\theta\rangle}{\partial x_3}\left(\frac{\partial\langle u_1\rangle}{\partial x_3}\right)^{-1} \tag{6}
$$

Figure 8 exhibits the profile of the turbulent Prandtl number versus the wall unit distance from the DNS simulations performed for $P_r = 1$. The turbulent Prandtl number reaches a decreasing asymptotic behavior close to unity except in the immediate vicinity of the wall where occurs a deviation from the asymptote. This result validates the hypothesis of an approximately constant turbulent Prandtl number with and without wall scalar fluctuations roughly around unity away from the wall.

5 Time-scale ratio $\mathcal{R} = (k_\theta\epsilon)/(k\epsilon_\theta)$

It is advantageous for engineering applications to compute the passive scalar to dynamic time-scale ratio $\mathcal{R} = (k_\theta\epsilon)/(k\epsilon_\theta)$ to get an estimate of the dissipation-rate $\epsilon_\theta = (k_\theta\epsilon)/(\mathcal{R}k)$. Figure 9 describes the evolution of this ratio $\mathcal{R}$ for the Prandtl numbers $P_r = 1$ versus the wall unit. It is found that $\mathcal{R}$ is not a universal constant but is a function of the wall unit distance. For both cases, it gradually decreases from high to low values in the near wall region and reaches a common asymptotic value when moving away from the wall. As the dissipation-rate ϵ_θ is close to zero at the wall for case II, $\mathcal{R}$ takes on extremely high values at $x_3 = 0$ in comparison with its corresponding values obtained for case I. Physically, this observation means that the time scale of the dynamic turbulent field k/ϵ differs from the time scale of the passive scalar field k_θ/ϵ_θ and that in the very near wall region the use of $\mathcal{R}$ is physically not relevant in practice for modeling closures.

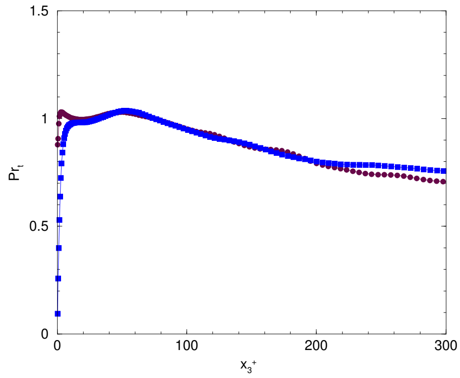

Figure 8: Profiles of the turbulent Prandtl number versus the wall unit distance. $\theta'_w = 0$ (case I), •. $q'_w = 0$ (case II), ■ $P_r = 1$; $R_\tau = 395$.

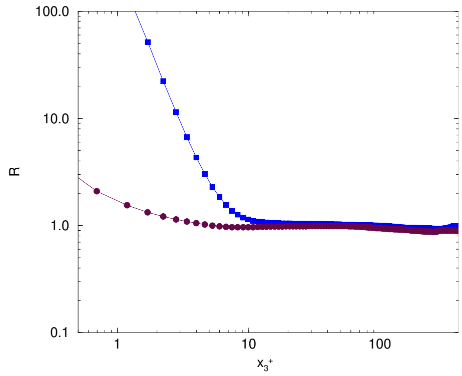

Figure 9: Dimensionless ratio $\mathcal{R} = (k_\theta \epsilon)/(k \epsilon_\theta)$ in logarithmic coordinate versus the wall unit distance. $\theta'_w = 0$ (case I), •. $q'_w = 0$ (case II), ■ $P_r = 1$; $R_\tau = 395$.

6 Conclusion and perspective

Direct numerical simulations of turbulent channel flow with scalar transport have been performed on different meshes for $R_\tau = 395$ and $P_r = 0.1$, 1 and 10. This work provides a useful high resolution DNS database (Chaouat, 2023). The budget of the transport equations for the scalar variance k_θ^+ and the streamwise turbulent flux $\tau_{1\theta}^+$ were obtained and the effect of the Prandtl number was investigated for case II in comparaison with case I. It has been found that the budget for k_θ^+ is largely dominated by the production and the dissipation terms that balance each other at all Prandtl numbers, whereas the molecular and turbulent diffusion terms are effective in the vicinity of the wall. The dissipation-rate ϵ_θ^+ and the molecular diffusion d_θ^+ terms are highly modified in the vicinity of the wall depending on the wall scalar boundary condition. As for k_θ^+, the budget for $\tau_{1\theta}^+$ is mainly controlled by the production term $P_{1\theta}^{+(1)}$ and the dissipation-rate term $\epsilon_{1\theta}^+$ away from the wall but the diffusion terms $d_{1\theta}^+$ and $T_{1\theta}^+$ are however appreciable in the vicinity of the wall. The dissipation and molecular diffusion terms are highly influenced by the wall scalar fluctuations but not the scalar-pressure gradient term $\Pi_{1\theta}^+$. In contrast to the budget for $\tau_{1\theta}^+$, the budget for $\tau_{3\theta}^+$ highly depends on the Prandtl number and is essentially governed by the production term $P_{3\theta}^+$, the dissipation term $\epsilon_{3\theta}^+$ but also the scalar-pressure gradient correlation term $\Pi_{3\theta}^+$. No substantial perceptible differences are observed for the budget $\tau_{3\theta}^+$ with respect to the wall boundary condition. The computations of the turbulent Prandtl-number Pr_t and the passive scalar to dynamic time-scale ratio $\mathcal{R}$ were performed at $P_r = 1$. These results show that accounting for wall scalar fluctuations should be considered in numerical simulations of turbulent flows involving fluid and solid combinations at the interface.

References

Chaouat, B. (2011). An efficient numerical method for RANS/LES turbulent simulations using subfilter scale stress transport equations. Int. J. Numer. Methods Fluids, Vol. 67, pp. 1207-1233.

Chaouat, B. (2017). The state of the art of hybrid RANS/LES modeling for the simulation of turbulent flows. Flow, Turbul. Combust., Vol. 99, pp. 279-327.

Chaouat, B. (2023). Contribution of direct numerical simulations to the budget and modelling of the transport equations for passive scalar turbulent fields with wall scalar fluctuations. J. Fluid Mech., Vol. 963, pp. 1-41.

Chaouat, B. and Peyret, C. (2019). Investigation of the wall scalar fluctuations effect on passive scalar turbulent fields at several Prandtl numbers by means of direct numerical simulations. J. Heat Transfer, ASME, Vol. 141, pp. 1-9.

Flageul, C., Benhamadouche, S., Lamballais E. and Laurence, D. (2015). DNS of turbulent channel flow with conjugate heat transfer: Effect of thermal boundary condition on the second moments and budgets. Int. J. Heat Fluid Flow, Vol. 55, pp. 34-44.

Hanjalic, K. and Launder, B.E. (2011). Modelling turbulence in engineering and the environnement. Second-moment route to closure. Cambridge University Press.

Kasagi, N., Kuroda, A. and Hirata, M. (1989). Numerical investigation of near-wall turbulent heat transfer taking into account the unsteady heat conduction in the solid wall. J. Heat Transfer, ASME, Vol. 111, pp. 385-392.

Kozuka, M., Seki, Y. and Kawamura, H. (2009). DNS of turbulent heat transfer in a channel flow with a high spatial resolution. Int. J. Heat Fluid Flow Vol. 30, pp. 514-524.

Schiestel, R. (2008). Modeling and simulation of turbulent flows. ISTE Ltd and J. Wiley.

Schiestel, R. and Chaouat, B. (2022). Turbulence modeling and simulation advances in CFD during the past 50 years. C. R. Acad. Sci. Paris Vol. 114, pp. 1-28.

Tennekes, H. and Lumley, J.L. (1972). A First Course in Turbulence, the MIT Press.

Tiselj, I., Pogrebnyak, E., Li, C., Mosyak, A. and Hetsroni, G. (2001). Effect of wall boundary condition on scalar transfer in a fully developed turbulent flume. Phys. Fluids, Vol. 13, pp. 1028-1039.